

COLOCATED MILLIMETER-WAVE RADARS:  
ALGORITHMS AND PERFORMANCE ANALYSIS

by

ASHWIN BHOBANI BARAL, BTech

DISSERTATION PROPOSAL

Presented to the Faculty of  
The University of Texas at Dallas  
in Partial Fulfillment  
of the Requirements  
for the Degree of

DOCTOR OF PHILOSOPHY IN  
ELECTRICAL ENGINEERING

THE UNIVERSITY OF TEXAS AT DALLAS  
April 2021

COLOCATED MILLIMETER-WAVE RADARS:  
ALGORITHMS AND PERFORMANCE ANALYSIS

Ashwin Bhabani Baral, PhD  
The University of Texas at Dallas, 2021

Supervising Professor: Murat Torlak, Chair

Millimeter-wave (mmWave) radars offer range accuracy in the sub-millimeter range by utilizing the larger available bandwidth in the frequency range 30 GHz - 300 GHz. Along with this high range accuracy, several mmWave sensing applications desire high angular resolution. To meet this requirement, mmWave radar with multiple-input multiple-output (MIMO) sensors systems are deployed. This dissertation proposal focuses on the signal processing algorithms for estimating the range, Doppler frequency and direction of arrival (DOA) of far-field targets, and their performance analysis.

Super-resolution algorithms like MULTiple SIgnal Classification (MUSIC) have been proposed for better direction of arrival (DOA) estimation performance as compared to classical approaches. MUSIC relies on accurate partitioning of the eigenvectors of the spatial correlation matrix between the signal (i.e., signal subspace) and noise eigenvectors (i.e., noise subspace). In this dissertation proposal, we present a novel statistical framework for analyzing the resolution performance of the MUSIC algorithm, in resolving two closely spaced targets, according to the number of noise eigenvectors used. Using this framework, we derive an analytical expression for the probability of resolution of the MUSIC algorithm. More importantly, real radio-frequency (RF) experiments are carried out to demonstrate the resolution performance of MUSIC to support our findings in practical settings.

The high angular resolution of MIMO radar comes at the expense of certain limitations of MIMO radar systems realized using different multiplexing techniques such as time division multiplexing (TDM), frequency division multiplexing (FDM) and code division multiplexing (CDM). The latter part of this dissertation proposal focuses on a problem associated with a standard TDM MIMO radar. In a standard TDM MIMO radar, transmitters are activated sequentially according to their natural spatial order. The drawback of the standard TDM MIMO approach is the coupling of velocity and DOA information of the targets. The coupling reduces the unambiguous estimation interval of the Doppler frequencies of the targets by the number of transmit antennas being multiplexed. To solve this problem, a signal processing approach will be presented in the dissertation.

Finally, we describe an interference problem associated with automotive radars most likely in a dense traffic scenario as the transmissions of automotive radars are not synchronized.

## TABLE OF CONTENTS

ABSTRACT . . . . .	ii
LIST OF FIGURES . . . . .	v
CHAPTER 1 INTRODUCTION . . . . .	1
CHAPTER 2 MUSIC ALGORITHM: PERFORMANCE ANALYSIS . . . . .	5
2.1 Signal Model . . . . .	5
2.2 MUSIC Algorithm . . . . .	6
2.3 Perturbation Model . . . . .	7
2.4 Resolution Criteria . . . . .	9
2.5 Derivation Framework . . . . .	11
2.6 Threshold SNR . . . . .	12
CHAPTER 3 PERFORMANCE ANALYSIS OF MUSIC: SIMULATION AND EXPERIMENTAL RESULTS . . . . .	14
3.1 Simulation Results . . . . .	14
3.1.1 Two Targets . . . . .	14
3.1.2 Three Targets . . . . .	21
3.2 Experimental Results . . . . .	22
CHAPTER 4 TDM MIMO RADAR . . . . .	28
4.1 FMCW Signal . . . . .	28
4.2 TDM MIMO: Signal Model . . . . .	29
4.3 Doppler Ambiguity Problem . . . . .	30
4.4 Proposed Idea . . . . .	32
CHAPTER 5 INTERFERENCE MITIGATION IN AUTOMOTIVE RADARS . . . . .	34
5.1 Problem Description . . . . .	34
CHAPTER 6 SUMMARY . . . . .	35
REFERENCES . . . . .	37
BIOGRAPHICAL SKETCH . . . . .	39

## LIST OF FIGURES

3.1 Comparison of probability of resolution curves obtained using simulations and analytical expression in [2] for two uncorrelated and equal-power sources when $M = 1$ . These curves are valid for target DOAs that are determined using (3.5) and (3.6) for any value of $\theta_m \in [-25^0, 25^0]$ with $\Delta\theta = 2^0$ . . . . .	16
3.2 Comparison of probability of resolution curves obtained using simulations and analytical expression in [2] for two uncorrelated and equal-power targets when $M = 6$ . These curves are valid for target DOAs that are determined using (3.5) and (3.6) for any value of $\theta_m \in [-25^0, 25^0]$ with $\Delta\theta = 2^0$ . . . . .	17
3.3 Analytical probability of resolution curves plotted for two uncorrelated and equal power targets with their respective DOA $13^0$ and $15^0$ when $M=2,3,6$ . . . . .	19
3.4 Simulated probability of resolution curves plotted for two uncorrelated and equal power targets with their respective DOA $13^0$ and $15^0$ . These curves are plotted for different number of noise eigenvector estimates i.e. $M = \{1, 2, 3, 4, 5, 6\}$ . . . . .	20
3.5 Analytical probability of resolution curves plotted for two uncorrelated and equal power targets located at $13^0$ and $15^0$ respectively for different values of $M$ , when different number of targets are involved ( $K = 2$ and $K = 3$ ). (Note: (A) indicates the resolution probability curve obtained analytically using the expression in [2] , whereas (S) indicates the curves are obtained through simulations.) . . . . .	22
3.6 24 GHz antenna array of INRAS Radarbook with 2 Tx and 8 Rx antennas . . . . .	23
3.7 A scenario from the experimental setup with two corner reflectors and INRAS radarbook . . . . .	24
3.8 Resolution performance of INRAS Radarbook by varying the number of noise subspace eigenvector estimates used across each different angle of separation between two reflectors . . . . .	25
3.9 Resolution performance of INRAS Radarbook by varying the number of the estimated noise subspace eigenvectors used in MUSIC spectrum computation with respect to varying radar transmit power level. . . . .	26
4.1 An example of a standard TDM MIMO radar with two transmit antenna elements. Frequency modulated continuous wave (FMCW) signals are assumed. . . . .	30
4.2 Doppler estimation using the standard TDM MIMO radar with $N_T = 2$ . . . . .	31

# CHAPTER 1

## INTRODUCTION

In recent years, mmWave radars have become popular with numerous sensing applications such as automotive radar, building security, human vital signs detection and people counting. The high resolution requirements of these applications are met through availability of larger bandwidth, better phase sensitivity and smaller size of antenna elements at mmWave frequencies. For applications desiring high angular resolution, mmWave radar sensors with MIMO principle are used.

Target localization is the essential functionality of a radar system in mmWave sensing applications. On receiving the echoes from targets, it estimates their parameters such as range, Doppler velocity and DOA. In the literature, several signal processing algorithms have been developed for the robust estimation of the parameters of multiple targets. Also, their performance analysis have been studied. However, there are certain investigations on the performance analysis of the existing algorithms that have been still missing. Or, there are some parameter estimation problems that have not yet been completely addressed. We attempt to address some of them in this dissertation proposal for far-field targets case.

Several automotive and industrial applications require better DOA estimation performance as they suffer due to low resolution performance of the classical approach. To address this case, super-resolution algorithm like MUSIC have been proposed in the literature. The resolution performance of the MUSIC algorithm has been studied extensively in the literature [23, 11, 18, 19, 9, 8, 25, 5, 10, 4, 22, 7, 13, 1]. These studies primarily rely on accurate partitioning of the eigenvector matrix of the spatial correlation matrix between the signal eigenvectors (i.e., signal subspace) and noise eigenvectors (i.e., noise subspace). However, the exact estimation of signal subspace size has been shown to be very critical [7]. As noted in many investigations such as [22], [7], inaccurate estimation of signal subspace size severely

degrades the spectral resolution of MUSIC. This has motivated the current work, i.e., analyzing the impact of number of noise eigenvectors on the resolution performance of MUSIC under the condition that two targets are closely spaced.

The probability of resolution is considered as an important statistical performance criterion of the MUSIC algorithm. Zhang in [23] was probably the first author who has explicitly derived a probability of resolution expression based on the statistical distribution of the criterion function. Later, Ferreól in [5] extended Zhang's resolution definition to investigate the MUSIC behavior in presence of model mismatches (calibration errors, etc.). The most existing investigations such as the aforementioned ones analyze the resolution performance of MUSIC by formulating the problem based on the availability of the complete set of noise eigenvectors. As a result, they fail to provide a performance variation when the different number of estimated noise subspace vectors are computed. Therefore, in the first part of this dissertation proposal, we derive an analytical tool to predict the resolution performance of the MUSIC algorithm according to the number of noise eigenvectors are used in the spectrum computation.

Following the discussion on the resolution problem of two closely targets, we next address a parameter estimation problem associated with a MIMO radar. Several mmWave sensing applications deploy colocated MIMO sensor systems to achieve high angular resolution. The MIMO radar system offers high angular resolution through the virtual array concept. The virtual array is synthesized through the convolution of antenna locations of transmit and receive antenna elements in the MIMO radar system. This high angular resolution is achieved with fewer antenna elements and at a low cost as compared to a corresponding single-input multiple-output (SIMO) radar system.

The high angular resolution comes, however, at the expense of certain limitations of MIMO radar systems realized using different multiplexing techniques such as time division multiplexing (TDM), frequency division multiplexing (FDM) and code division multiplexing

(CDM). Of all these multiplexing techniques, TDM seems to be the appropriate choice for automotive applications due to its low hardware complexity [15, 16]. Also, the orthogonality of the radar waveforms is easily realized in TDM MIMO by activating only one transmitter at a time. In a standard TDM MIMO radar, the transmitters are activated according to their natural spatial order. Due to the relative motion between the radar and a target, an additional phase component, related to the Doppler velocity of the target, is induced in the phase sequences of the virtual antenna elements. With this additional phase component, the Doppler frequency is coupled with the direction of arrival (DOA) of the target in the received signals. The coupling of Doppler frequency and DOA information distorts the phase of the signals captured by virtual elements. As a result, the unambiguous Doppler estimation interval of a standard TDM MIMO radar is reduced by the number of transmit antenna elements as compared to the one in an equivalent SIMO radar. This is known as the Doppler ambiguity problem in TDM MIMO radar literature. To address this problem, a signal processing method will be presented in the dissertation.

The modern cars are equipped with automotive radars for developing automotive applications that are responsible for providing the drivers' safety and comfort features. Since the transmissions from automotive radars are not synchronized, the occurrence of interference is very likely in traffic environments involving dense target scenario. A signal processing will be proposed to reduce or mitigate the interference.

The rest of the dissertation proposal is organized as follows:

- Chapter 2 reviews MUSIC algorithm with a signal model, introduce a first-order perturbation expression of noise subspace for deriving the analytical expressions, presents derivation framework and resolution threshold analysis in terms of signal-to-noise ratio (SNR)

- Chapter 3 presents simulation results to verify the accuracy of the analytical expression and experimental results to demonstrate the resolution capability of MUSIC with variation of the number of noise eigenvectors used in the spectrum computation.
- Chapter 4 formulates the Doppler ambiguity problem associated with a standard TDM MIMO radar
- Chapter 5 describes the interference problem associated with automotive radars
- Chapter 6 summarizes the dissertation proposal

## CHAPTER 2

### MUSIC ALGORITHM: PERFORMANCE ANALYSIS

In this dissertation proposal, we investigate the resolution performance of MUSIC algorithm, in resolving two closely spaced targets, according to the number of noise eigenvectors used in the spectrum computation. In this chapter, we review the MUSIC algorithm with a signal model. We introduce a first-order perturbation model for noise subspace to derive the analytical expressions. Also, we discuss the derivation procedure and present the resolution threshold analysis in terms of signal-to-noise ratio (SNR).

#### 2.1 Signal Model

We consider the plane waves from  $K$  targets, having direction-of-arrivals (DOAs)  $\{\theta_n\}_{n=1,\dots,K}$ , incident upon an array of  $L$  ( $L > K$ ) antenna elements. Then, in an ideal environment, the received data samples of  $N$  successive snapshots can be represented in matrix form as

$$\mathbf{Y} = \mathbf{AS} \quad (2.1)$$

with a signal matrix  $\mathbf{S}$

$$\mathbf{S} = \left[ \mathbf{s}(1), \mathbf{s}(2), \dots, \mathbf{s}(N) \right] \quad (2.2)$$

$$\mathbf{s}(m) = \left[ s_1(m), s_2(m), \dots, s_K(m) \right]^T \quad m = 1, 2, \dots, N \quad (2.3)$$

and a steering matrix  $\mathbf{A}$

$$\mathbf{A} = \left[ \mathbf{a}(\theta_1), \mathbf{a}(\theta_2), \dots, \mathbf{a}(\theta_K) \right]. \quad (2.4)$$

In case of a uniform linear array, we can express each steering vector as

$$\mathbf{a}(\theta_n) = \left[ 1, e^{-jkd \sin(\theta_n)}, \dots, e^{-j(L-1)kd \sin(\theta_n)} \right]^T \quad (2.5)$$

where  $n = 1, 2, \dots, K$ ,  $(.)^T$  denotes the transpose,  $s_n(m)$  is a narrowband signal received from  $n$ th target at the  $m$ th snapshot,  $k$  denotes the wavenumber, and  $d$  is the inter-element

spacing between antenna elements in the array. The received data matrix  $\mathbf{Y}$ , observed without noise, is random if the signal vector  $\mathbf{s}(m)$  is distributed as a  $K$ -dimensional complex Gaussian vector with zero mean and a covariance matrix of  $\mathbf{R}_S$ .

## 2.2 MUSIC Algorithm

The MUSIC algorithm relies on accurate partitioning of the eigenvectors of the spatial correlation matrix between the signal (i.e., signal subspace) and noise eigenvectors (i.e., noise subspace). The eigenvectors can be obtained by an eigenvalue decomposition (EVD) of the data covariance matrix

$$\hat{\mathbf{R}} = \frac{1}{N} \mathbf{Y} \mathbf{Y}^H = \begin{bmatrix} \mathbf{U}_s & \mathbf{U}_o \end{bmatrix} \begin{bmatrix} \Sigma_s^2 & \mathbf{0} \\ \mathbf{0} & \mathbf{0} \end{bmatrix} \begin{bmatrix} \mathbf{U}_s^H \\ \mathbf{U}_o^H \end{bmatrix} \quad (2.6)$$

or by the singular value decomposition (SVD) of the received data matrix  $\mathbf{Y}$ :

$$\mathbf{Y} = \mathbf{U} \Sigma \mathbf{V}^H = \begin{bmatrix} \mathbf{U}_s & \mathbf{U}_o \end{bmatrix} \begin{bmatrix} \Sigma_s & \mathbf{0} \\ \mathbf{0} & \mathbf{0} \end{bmatrix} \begin{bmatrix} \mathbf{V}_s^H \\ \mathbf{V}_o^H \end{bmatrix} \quad (2.7)$$

where  $\mathbf{U}_s$  and  $\mathbf{U}_o$  represent the signal and the orthogonal subspaces, respectively and  $(\cdot)^H$  denotes the Hermitian transpose. Generally, the orthogonal subspace is referred as the noise subspace. However, as discussed in [12], the orthogonal complement of the signal subspace is aptly referred as the orthogonal subspace for the problem where a noise-free data model is used. The vectors in  $\mathbf{U}_s$  are associated with  $K$  singular values in  $\Sigma_s$  whereas the vectors in  $\mathbf{U}_o$  are associated with zero singular values. The left singular vectors obtained from the SVD of data matrix  $\mathbf{Y}$  are same as the eigenvectors obtained from eigenvalue decomposition (EVD) of the sample data covariance matrix. Henceforth, we refer the column vectors of  $\mathbf{U}$  as eigenvectors.

Let the vectors  $\{\mathbf{u}_k\}$ ,  $k = 1, 2, \dots, L$  represent the complete set of column vectors of the matrix  $\mathbf{U}$ . We can partition these vectors into signal subspace and orthogonal subspace as

follows

$$\mathbf{U} = \left[ \mathbf{u}_1, \mathbf{u}_2, \dots, \mathbf{u}_L \right] \quad (2.8)$$

$$\mathbf{U}_s = \left[ \mathbf{u}_1, \dots, \mathbf{u}_K \right] \quad \text{and} \quad \mathbf{U}_o = \left[ \mathbf{u}_{K+1}, \dots, \mathbf{u}_L \right]. \quad (2.9)$$

The number of eigenvectors spanning signal and orthogonal subspaces are  $K$  and  $L - K$ , respectively.

Let  $M$  represent the number of orthogonal eigenvectors used in the MUSIC spectrum computation, then its spatial pseudo-spectrum can be expressed as

$$S_M(\theta) = \frac{1}{\mathbf{a}^H(\theta) \left( \sum_{k=K+1}^{K+M} \mathbf{u}_k \mathbf{u}_k^H \right) \mathbf{a}(\theta)} \quad (2.10)$$

$M$  varies from 1 to  $L - K$ . It is convenient to analyze the resolution performance of MUSIC statistically using its null spectrum. The expression of the null spectrum is obtained by the inverse of its psuedo-spectrum.

$$P_M(\theta) = \frac{1}{S_M(\theta)} = \mathbf{a}^H(\theta) \left( \sum_{k=K+1}^{K+M} \mathbf{u}_k \mathbf{u}_k^H \right) \mathbf{a}(\theta) \quad (2.11)$$

In the presence of the measurement noise, the spectrum estimation above cannot be perfect. As noted in many investigations such as [22], [7], inaccurate estimation of signal subspace size severely degrades the MUSIC spectrum especially when DOAs are closely spaced. Our work will analyze the impact of number of noise eigenvectors on the resolution performance of MUSIC under the condition that two DOAs are closely spaced. Also, we will analyze the resolution performance of MUSIC for resolving two closely spaced targets in presence of other targets.

### 2.3 Perturbation Model

The fidelity of sample data covariance matrix can deviate from the true covariance matrix due to finite data effect, measurement noise, and modeling errors. Inaccurate sample data

covariance matrix will lead to erroneous estimation of signal and noise subspaces by the subspace decomposition. In this dissertation proposal, we consider the first order perturbation of the noise subspace vectors due to measurement noise and finite sample sizes. Thus, the received data samples in noisy environment can be expressed as

$$\hat{\mathbf{Y}} = \mathbf{Y} + \mathbf{W} \quad (2.12)$$

where the measurement noise  $\mathbf{W}$  is modeled as an additive white Gaussian noise. The elements of  $\mathbf{W}$  are independent and identically distributed complex Gaussian random variables with mean zero and variance  $\sigma_w^2$ . Using the relation in (2.1), we can rewrite (2.12) as

$$\hat{\mathbf{Y}} = \mathbf{AS} + \mathbf{W} \quad (2.13)$$

where the signals  $\mathbf{S}$  and the noise  $\mathbf{W}$  are independent.

The SVD of the noisy received data matrix is given by

$$\hat{\mathbf{Y}} = \hat{\mathbf{U}}\hat{\Sigma}\hat{\mathbf{V}}^H = \begin{bmatrix} \hat{\mathbf{U}}_s & \hat{\mathbf{U}}_o \end{bmatrix} \begin{bmatrix} \hat{\Sigma}_s & \mathbf{0} \\ \mathbf{0} & \hat{\Sigma}_o \end{bmatrix} \begin{bmatrix} \hat{\mathbf{V}}_s^H \\ \hat{\mathbf{V}}_o^H \end{bmatrix} \quad (2.14)$$

where  $\hat{\mathbf{U}}_s$  and  $\hat{\mathbf{U}}_o$  represent the estimated signal and orthogonal subspaces respectively. As we are dealing with the perturbations due to measurement noise in this dissertation proposal, we refer the orthogonal subspace estimate as the estimated noise subspace and correspondingly the vectors in  $\hat{\mathbf{U}}_o$  as the estimated noise eigenvectors. The perturbation in the sample data covariance matrix due to noise results in the perturbations of the signal and orthogonal subspace through SVD.

The estimated signal and noise subspaces can be expressed as

$$\hat{\mathbf{U}}_s = \mathbf{U}_s + \Delta\mathbf{U}_s \quad (2.15)$$

$$\hat{\mathbf{U}}_o = \mathbf{U}_o + \Delta\mathbf{U}_o \quad (2.16)$$

where  $\Delta \mathbf{U}_s$  and  $\Delta \mathbf{U}_o$  represent the perturbations in the estimated signal and noise subspaces, respectively. In this dissertation proposal, the computation of the null spectrum is associated with the estimated noise subspace. Therefore, we need an analytical expression for the perturbation of the noise subspace in order to analyze the statistical resolution performance of MUSIC given the number of noise eigenvectors. To derive an analytical expression for the resolution performance of MUSIC, we leverage the first-order perturbation expressions obtained in [11] for the perturbation of the noise subspace.

$$\Delta \mathbf{U}_o = -\mathbf{U}_s \boldsymbol{\Sigma}_s^{-1} \mathbf{V}_s^H \mathbf{W}^H \mathbf{U}_o \quad (2.17)$$

The parameters  $\mathbf{U}_s$ ,  $\mathbf{U}_o$ ,  $\mathbf{V}_s$  and  $\boldsymbol{\Sigma}_s$  in (2.17) are obtained from the SVD of the noise-free received data  $\mathbf{Y}$ . In order to analyze the impact of the number of noise eigenvectors on the resolution performance of MUSIC, let the vectors  $\{\hat{\mathbf{u}}_k\}_{k=K+1,\dots,L}$  denote the eigenvectors from the estimated noise subspace as

$$\hat{\mathbf{u}}_k = \mathbf{u}_k + \delta \mathbf{u}_k, \quad k = K + 1, \dots, L \quad (2.18)$$

where  $\delta \mathbf{u}_k$  represents the perturbation of the orthogonal subspace eigenvector  $\mathbf{u}_k$ . Then, the first-order expression for the perturbation of orthogonal subspace eigenvector due to perturbations in data is given as

$$\delta \mathbf{u}_k = -\mathbf{U}_s \boldsymbol{\Sigma}_s^{-1} \mathbf{V}_s^H \mathbf{W}^H \mathbf{u}_k, \quad k = K + 1, \dots, L \quad (2.19)$$

From the above expression, we can easily show that the perturbation ( $\delta \hat{\mathbf{u}}_k$ ) of orthogonal subspace eigenvector ( $\mathbf{u}_k$ ) is a multivariate complex Gaussian process as it is a linear transformation of complex Gaussian noise  $\mathbf{W}$ .

## 2.4 Resolution Criteria

In order to determine whether MUSIC can resolve any two closely spaced targets or not, a decision criterion is needed. We select the criterion defined in [25] when the MUSIC

pseudo-spectrum exhibit two peaks close to the true DOAs. The corresponding resolution test statistics is represented by a variable  $\gamma_M$  where  $M$  is the number of noise eigenvectors used in the MUSIC estimator. The expression for  $\gamma_M$  is written in a similar manner as given in [23].

$$\gamma_M = \frac{1}{2} \left\{ \hat{P}_M(\theta_1) + \hat{P}_M(\theta_2) \right\} - \hat{P}_M(\theta_m) \quad (2.20)$$

with

$$\theta_m = \frac{\theta_1 + \theta_2}{2} \quad (2.21)$$

where  $\theta_m$  denotes the mean value angle of the two target DOAs  $\theta_1$  and  $\theta_2$ .  $\hat{P}_M(\theta_1)$ ,  $\hat{P}_M(\theta_2)$  and  $\hat{P}_M(\theta_m)$  represent the estimated null spectrum at the DOAs  $\theta_1$ ,  $\theta_2$  and  $\theta_m$ , respectively. The two targets are considered as resolved if the estimated null spectrum at  $\theta_m$  is greater than the average of the null spectrum estimates at  $\theta_1$  and  $\theta_2$  or otherwise they are considered as unresolved.

Using the definition of the estimated null spectrum in (2.20), we obtain an expression for  $\gamma_M$  as

$$\gamma_M = \frac{1}{2} \left\{ \sum_{k=K+1}^{K+M} \mathbf{a}_1^H \hat{\mathbf{u}}_k \hat{\mathbf{u}}_k^H \mathbf{a}_1 + \sum_{k=K+1}^{K+M} \mathbf{a}_2^H \hat{\mathbf{u}}_k \hat{\mathbf{u}}_k^H \mathbf{a}_2 \right\} - \sum_{k=K+1}^{K+M} \mathbf{a}_m^H \hat{\mathbf{u}}_k \hat{\mathbf{u}}_k^H \mathbf{a}_m \quad (2.22)$$

with

$$\mathbf{a}_l = \mathbf{a}(\theta_l) \quad l = 1, 2, m \quad (2.23)$$

where  $\mathbf{a}_1$ ,  $\mathbf{a}_2$  and  $\mathbf{a}_m$  represent the steering vectors for the locations  $\theta_1$ ,  $\theta_2$  and  $\theta_m$  respectively. Using the inequality expression involving  $\gamma_M$  for the resolved case as in [23], we can write the probability of resolution expression as

$$P_{R_M} = P [\gamma_M < 0]. \quad (2.24)$$

As reported in literature [5], there are different condition tests which are different approximations of the decision test used here. Our goal is to demonstrate the effectiveness of our

approach with the most commonly used test in the literature. Towards that goal, we obtain the characteristic function of the test statistics  $\gamma_M$  in terms of any given set of noise eigenvectors.

## 2.5 Derivation Framework

The derivation of the probability of resolution expression is carried out in multiple steps. We first derive an analytical expression for the characteristic function of the random decision variable  $\gamma_M$ . This decision variable is expressed as a quadratic form in complex Gaussian random vectors. Following this, we determine the probability density function (PDF) of  $\gamma_M$  from its characteristic function. Finally, we derive the expression for probability of resolution of MUSIC algorithm using the PDF.

An analytical expression for the characteristic function of  $\gamma_M$  is derived leveraging the results in [23] and [24]. First, we determine the characteristic function of the decision variable per estimated noise eigenvector. Let  $\gamma_{M_k}$  represent the decision variable corresponding to the estimated noise eigenvector  $\hat{\mathbf{u}}_k$  when  $M$  noise eigenvector estimates are used.

$$\gamma_{M_k} = \frac{1}{2} \left\{ \mathbf{a}_1^H \hat{\mathbf{u}}_k \hat{\mathbf{u}}_k^H \mathbf{a}_1 + \mathbf{a}_2^H \hat{\mathbf{u}}_k \hat{\mathbf{u}}_k^H \mathbf{a}_2 \right\} - \mathbf{a}_m^H \hat{\mathbf{u}}_k \hat{\mathbf{u}}_k^H \mathbf{a}_m \quad k = K+1, \dots, L \quad (2.25)$$

From (2.22) and (2.25), we can express  $\gamma_M$  as

$$\gamma_M = \sum_{k=K+1}^{K+M} \gamma_{M_k} \quad (2.26)$$

Using the standard expression of the characteristic function of hermitian quadratic forms in complex normal random variables from [21], we obtain the expression of the characteristic function  $\phi_{\gamma_{M_k}}(t)$  of  $\gamma_{M_k}$  with some simplifications in [2]. Since the noise eigenvector estimates are statistically independent and identically distributed, the characteristic function of  $\gamma_M$  is obtained in (2.27) using the expression in (2.26).

$$\phi_{\gamma_M}(t) = E[\exp(j\gamma_M t)] = E\left[\exp\left(\sum_{k=K+1}^{K+M} j\gamma_{M_k} t\right)\right] = \prod_{k=K+1}^{K+M} \phi_{\gamma_{M_k}}(t) \quad (2.27)$$

We determine the PDF of the decision variable  $\gamma_M$  using the characteristic function obtained in [2]

$$p_{\gamma_M}(y) = \frac{1}{2\pi} \int_{-\infty}^{\infty} \phi_{\gamma_M}(t) \exp(-jyt) dt \quad (2.28)$$

The expression of the probability of resolution of MUSIC algorithm, when  $M$  noise eigenvector estimates are used, is given as

$$P_{R_M} = P[\gamma_M < 0] = \int_{-\infty}^0 p_{\gamma_M}(y) dy \quad (2.29)$$

The expressions of the PDF and the probability of resolution of  $\gamma_M$  are derived in [2].

## 2.6 Threshold SNR

It is well-known that the exact estimate of signal subspace size is extremely critical in low SNR cases. Thus, the MUSIC algorithm, which relies primarily on the accurate partitioning of sample space into signal subspace and noise subspace, offers low resolution performance in such cases. This low resolution performance of the MUSIC algorithm is associated with a phenomenon known as subspace swap, which occurs in the threshold region when a small portion of the true signal subspace is better represented by some portions of the estimated noise subspace than by some portions of the estimated signal subspace [20]. This motivated us to investigate the resolution performance of the MUSIC algorithm by varying the number of noise eigenvectors in the null spectrum computation. In fact, the expression in (??) can predict the resolution performance of MUSIC according to the number of noise eigenvectors used in the threshold region.

The drop in the resolution performance of the MUSIC algorithm is observed when the SNR falls below a threshold value [20]. For our investigation on the resolution performance of the MUSIC algorithm with the varying number of noise eigenvectors , we need to determine the threshold SNR value in order to identify the region of SNR for which the aforementioned

phenomenon occurs. Therefore, an analytical expression of the threshold SNR is desired. Using this expression, we perform the resolution threshold analysis according to the number of noise eigenvectors used in the null spectrum computation.

We determine the expression of the threshold SNR by taking an ensemble average of the null spectrum estimates in the threshold equation defined in [25].

$$E \left[ \hat{P}_M(\theta_m) \right] = \frac{1}{2} \left\{ E \left[ \hat{P}_M(\theta_1) \right] + E \left[ \hat{P}_M(\theta_2) \right] \right\} \quad (2.30)$$

From [8] and [10], it has been concluded that mean of the null spectrum estimate represents the statistical behavior of the null spectrum estimate as its variance is very small compared to its mean. Thus, the mean of the null spectrum estimate has been used to compute the threshold SNR and is computed as

$$\begin{aligned} E \left[ \hat{P}_M(\theta_j) \right] &= E \left[ \sum_{k=K+1}^{K+M} \mathbf{a}_j^H \hat{\mathbf{u}}_k \hat{\mathbf{u}}_k^H \mathbf{a}_j \right] \\ &= \sum_{k=K+1}^{K+M} \mathbf{a}_j^H \mathbf{u}_k \mathbf{u}_k^H \mathbf{a}_j + \frac{M\sigma_w^2 \mathbf{a}_j^H \mathbf{P} \mathbf{a}_j}{N} \end{aligned} \quad (2.31)$$

where

$$\mathbf{P} = \mathbf{A}^{H\dagger} \mathbf{R}_S^{-1} \mathbf{A}^\dagger \quad (2.32)$$

The expression in (2.31) is valid for  $j = 1, 2, m$ . Substituting (2.31) in (2.30), we get

$$\sum_{k=K+1}^{K+M} \mathbf{a}_m^H \mathbf{u}_k \mathbf{u}_k^H \mathbf{a}_m + \frac{M\sigma_{wc}^2 \mathbf{a}_m^H \mathbf{P} \mathbf{a}_m}{N} = \frac{M\sigma_{wc}^2}{2N} (\mathbf{a}_1^H \mathbf{P} \mathbf{a}_1 + \mathbf{a}_2^H \mathbf{P} \mathbf{a}_2) \quad (2.33)$$

where  $\sigma_{wc}^2$  denotes a particular value of noise power for which (2.33) is satisfied. In the dissertation proposal, we perform the resolution threshold analysis of the MUSIC algorithm for a case where two closely spaced targets ( $K = 2$ ) are involved. The expression of the resolution threshold SNR for MUSIC algorithm is derived in [2].

We present both simulation and experimental results for the resolution performance of MUSIC algorithm, when different number of noise or orthogonal eigenvectors are used, in the next chapter

# CHAPTER 3

## PERFORMANCE ANALYSIS OF MUSIC: SIMULATION AND EXPERIMENTAL RESULTS

In [2], we derive the analytical expressions to predict the probability of resolution and the resolution threshold SNR for MUSIC algorithm when different number of noise eigenvectors are used. In this chapter, simulation results are presented to verify the accuracy of the analytical expressions. Also, we demonstrate the resolution performance of MUSIC according to the number of noise eigenvectors through real radio-frequency (RF) experiments.

### 3.1 Simulation Results

We present the simulation results in this section to verify the accuracy of the probability of resolution expression and the threshold SNR expression in [2]. The results in this section discuss the resolution performance of MUSIC when different number of noise or orthogonal eigenvectors are used. Also, we analyze the resolution performance of MUSIC with different number of targets involved in the scenario.

#### 3.1.1 Two Targets

In this section, we discuss the simulation results for a case when only two closely spaced targets are involved. Our simulations consider a ULA of 8 elements ( $L = 8$ ) with an inter-element spacing of half-wavelength ( $d = \lambda/2$ ). The signals, arriving at ULA, from two targets ( $K = 2$ ) are modeled as zero mean complex Gaussian with the signal covariance matrix

$$\mathbf{R}_S = \begin{bmatrix} 1 & 0 \\ 0 & 1 \end{bmatrix} \quad (3.1)$$

Two targets are assumed to be uncorrelated and have equal power. This is applicable for all the simulations presented in this section. Also, we consider 100 successive snapshots

( $N = 100$ ) of the signals to be received at the array. The signals received at the array from two targets are perturbed by the measurement noise. The measurement noise is modeled as additive white Gaussian noise with noise power  $\sigma_w^2$ . Also, the Gaussian noise are assumed to be spatially uncorrelated. The SNR in all the results is associated with that of a target having DOA  $\theta_1$ . If  $\sigma_1^2$  represents the power of the target having DOA  $\theta_1$ , then we define the SNR as

$$\text{SNR} = 10 \log_{10} \left( \frac{\sigma_1^2}{\sigma_w^2} \right) \quad (3.2)$$

All the simulations are performed with 50,000 independent trials. These simulation results are evaluated by using the resolution condition as discussed in section 2.4. We summarize some parameters that are applicable for all simulations below.

$$L = 8, \quad d = \lambda/2 \quad (3.3)$$

$$K = 2, \quad N = 100 \quad (3.4)$$

The number of eigenvectors available in the orthogonal subspace as well as in the noise subspace estimate is 6 (i.e.  $L - K = 6$ ).

The values of the probability of resolution expression in [2] can be computed using the standard software packages such as Mathematica. Given the middle angle ( $\theta_m$ ) between two target DOAs ( $\theta_1 \& \theta_2$ ) and the target separation ( $\Delta\theta$ ), the target DOAs are computed as

$$\theta_1 = \theta_m - \Delta\theta/2 \quad (3.5)$$

$$\theta_2 = \theta_m + \Delta\theta/2 \quad (3.6)$$

where

$$\Delta\theta = \theta_2 - \theta_1 \quad (3.7)$$

The analytical results of the probability of resolution curves are confirmed with two cases. The first case is when only one orthogonal subspace eigenvector (i.e.  $M = 1$ ) is used in the

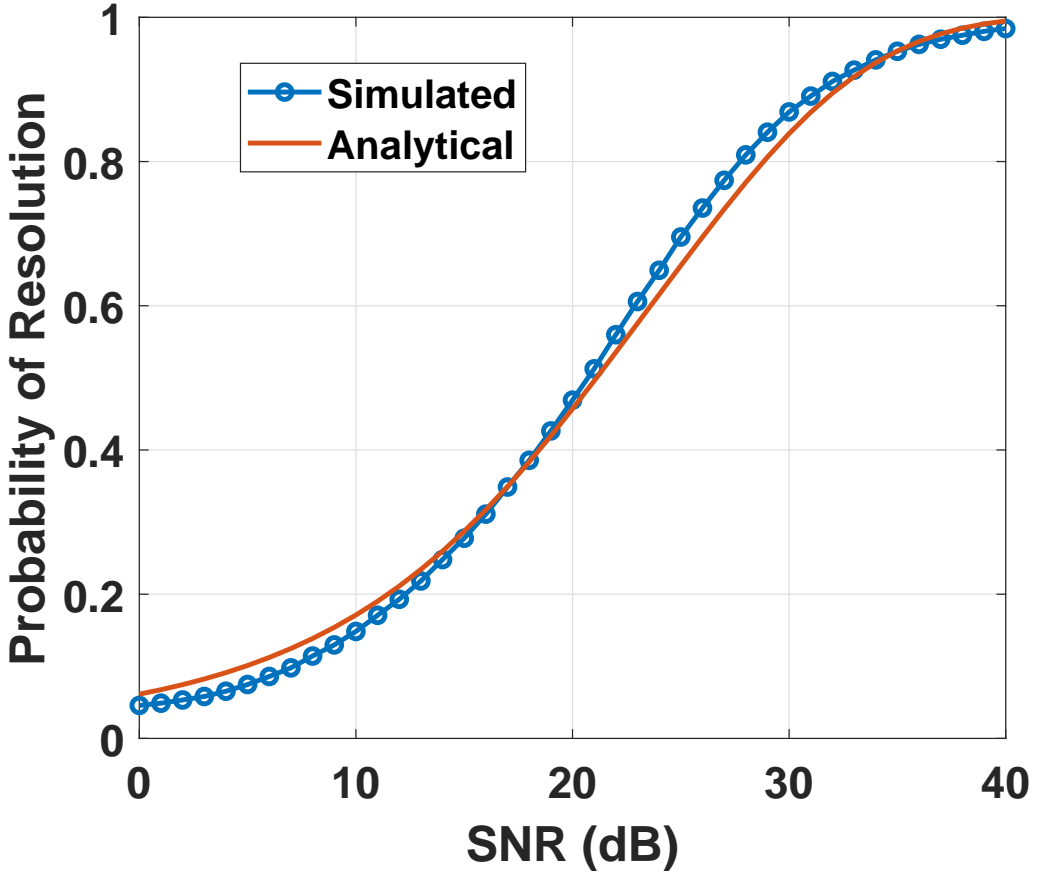


Figure 3.1. Comparison of probability of resolution curves obtained using simulations and analytical expression in [2] for two uncorrelated and equal-power sources when  $M = 1$ . These curves are valid for target DOAs that are determined using (3.5) and (3.6) for any value of  $\theta_m \in [-25^0, 25^0]$  with  $\Delta\theta = 2^0$

computation of null spectrum. The second case is when all orthogonal subspace eigenvectors (i.e.  $M = 6$ ) are used. First, we consider the case of using only one orthogonal subspace eigenvector. The simulated and analytical probability of resolution curves are plotted at different SNR in Fig. 3.1 when  $M = 1$ . These results are valid for target DOAs that are obtained using (3.5) and (3.6) for any value of  $\theta_m \in [-25^0, 25^0]$  with  $\Delta\theta = 2^0$ . In this case, the simulated curve is the mean of the probability of resolution curves obtained through 50,000 independent trials for different target directions. The different values of the target directions are determined by varying the value of  $\theta_m$  within the range  $[-25^0, 25^0]$

in (3.5) and (3.6) with  $\Delta\theta = 2^0$ . Also, the single noise eigenvector estimate corresponds to the eigenvector associated with smallest eigenvalue for all simulation trials. The single orthogonal subspace eigenvector in the analytical case is chosen randomly. For the analytical curve, the probability of resolution curves obtained for each orthogonal subspace eigenvector are averaged over all the orthogonal subspace eigenvectors. These curves are determined for two targets having DOAs  $\theta_1 = 3^0$  and  $\theta_2 = 5^0$ . Both the analytical and simulated curves are evaluated at each SNR for all cases presented in this section.

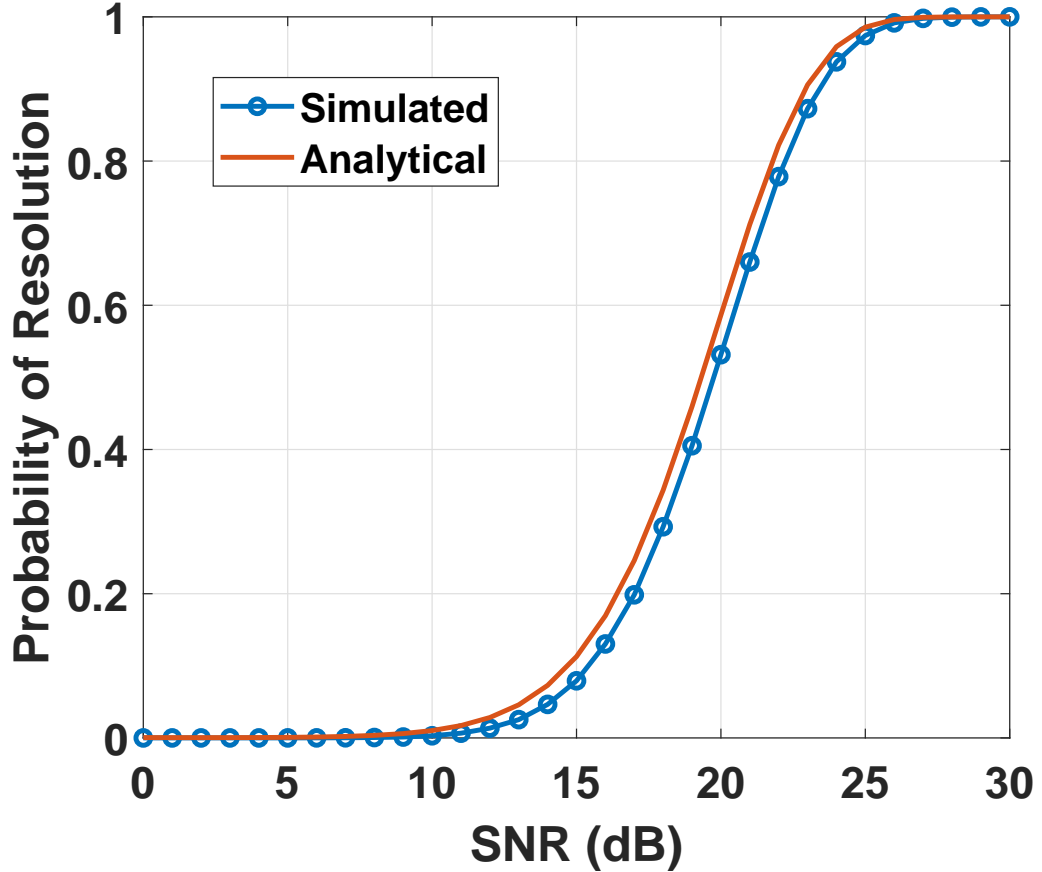


Figure 3.2. Comparison of probability of resolution curves obtained using simulations and analytical expression in [2] for two uncorrelated and equal-power targets when  $M = 6$ . These curves are valid for target DOAs that are determined using (3.5) and (3.6) for any value of  $\theta_m \in [-25^0, 25^0]$  with  $\Delta\theta = 2^0$

Fig. 3.2 compares the analytical and simulated probability of resolution curves at various SNR when  $M = 6$ . These curves are obtained for two uncorrelated targets whose DOAs are determined using (3.5) and (3.6) for any value of  $\theta_m \in [-25^0, 25^0]$  with  $\Delta\theta = 2^0$ . For this case, the analytical curve is obtained using the expression in [2] when  $M = 6$  for two target directions  $\theta_1 = 13^0$  and  $\theta_2 = 15^0$ . And, the simulated curve is the mean of the probability of resolution curves obtained through 50,000 independent trials for various target directions. These are determined using (3.5) and (3.6) for different values of  $\theta_m$  in the interval  $[-25^0, 25^0]$  with  $\Delta\theta = 2^0$ . From Fig. 3.1 and Fig. 3.2, it can be seen that the analytical curves approximately match the simulated curves. Thus, the accuracy of the probability of resolution expression in [2] is successfully verified.

The resolution performance of the MUSIC algorithm according to the number of noise eigenvectors used has so far been discussed for a particular value of  $M$ . In addition, we want to investigate how the probability of resolution behaves with the variation of the number of noise eigenvectors used in the null spectrum computation. Thus, three analytical probability of resolution curves are plotted in Fig. 3.3 with different SNR for  $M = \{2, 3, 6\}$ . The value of  $M$  indicates the number of orthogonal subspace eigenvectors that are used in the null spectrum computation. The curves in Fig. 3.3 are obtained using the expression in [2] for two uncorrelated targets at the locations  $13^0$  and  $15^0$ . In Fig. 3.3, we observe that MUSIC has better resolution performance when  $M = 2$  as compared to the cases when  $M = \{3, 6\}$  for low SNR values. Conversely, MUSIC has better resolution performance when  $M = 6$  as compared to the cases when  $M = \{2, 3\}$  for high SNR values. Since the probability of resolution curves in Fig. 3.3 crossover at a particular SNR value, we refer this particular value of SNR as the crossover SNR in this dissertation proposal. Thus, a trend is observed in the behavior of the probability of resolution with the variation of the number of noise eigenvectors used. Following this trend for the SNR values below the crossover SNR, we conclude that MUSIC can achieve better resolution performance when fewer number of

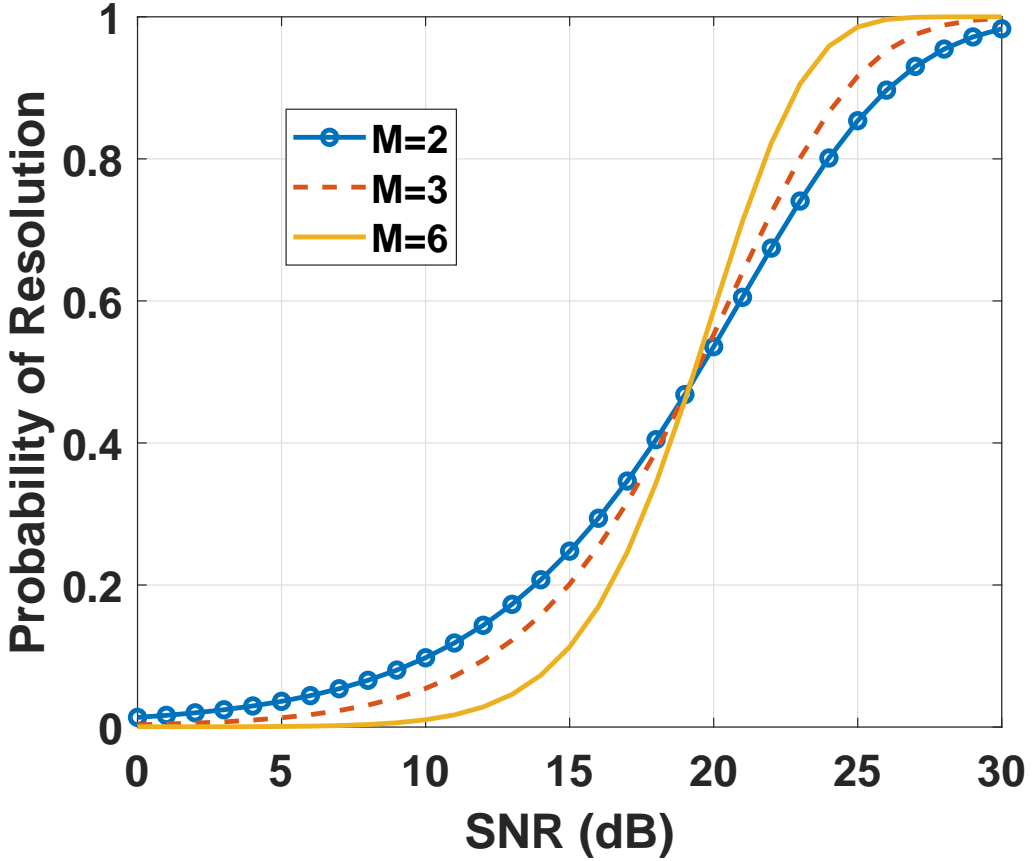


Figure 3.3. Analytical probability of resolution curves plotted for two uncorrelated and equal power targets with their respective DOA  $13^0$  and  $15^0$  when  $M=2,3,6$

noise eigenvectors ( $M < L - K$ ) are used as compared to the case when all the available ones ( $M = L - K$ ) are used. Conversely, for the SNR values above the crossover SNR, MUSIC can achieve better resolution performance when all the noise eigenvectors are used as compared to the case when fewer ones are used.

From Fig. 3.3, we can see that the value of the crossover SNR is approximately about 19dB. This value of crossover SNR is found to be approximately the same as the one computed using the analytical expression of the threshold SNR in [2]. We obtain the theoretical value of threshold SNR as 19.4dB. Thus, we can refer the threshold SNR as the crossover SNR. The parameters required for the computation of the threshold SNR using the expression in [2] are  $\sigma_1 = 1$ ,  $\sigma_2 = 1$ ,  $\theta_1 = 13^0$ ,  $\theta_2 = 15^0$ ,  $\theta_m = 14^0$ ,  $N = 100$  and  $\rho = 0$ . The

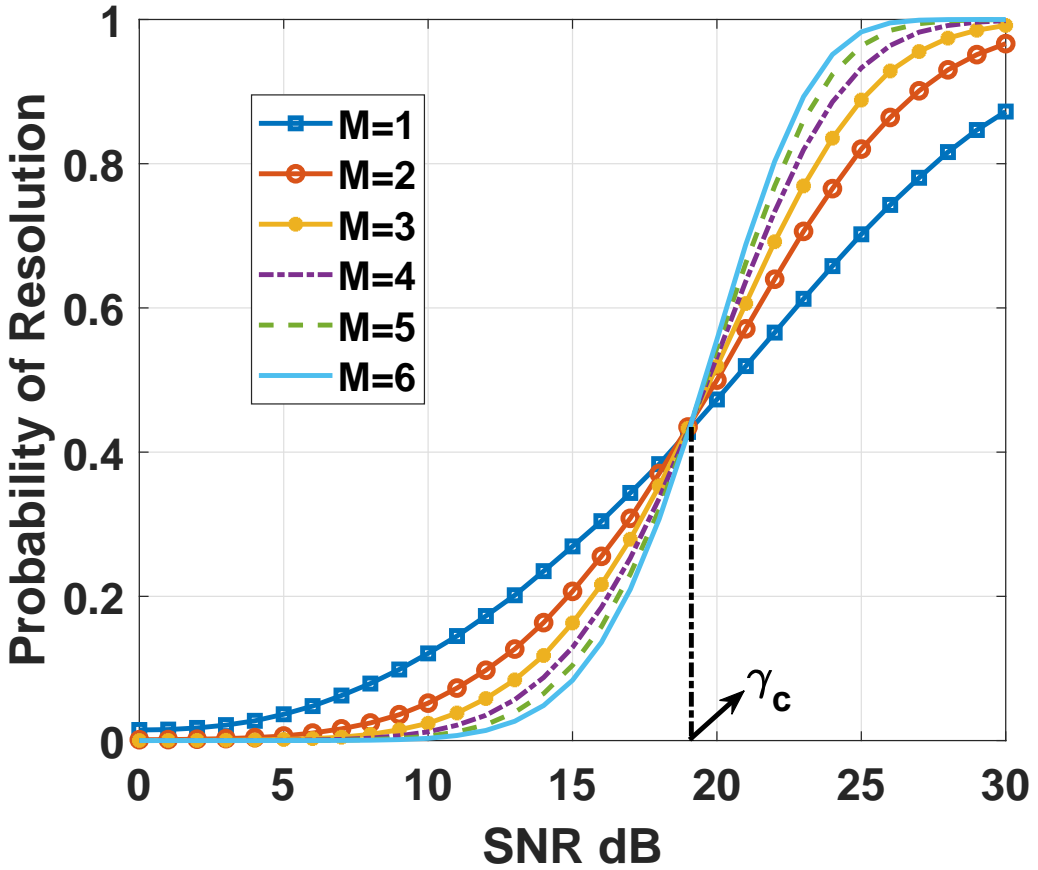


Figure 3.4. Simulated probability of resolution curves plotted for two uncorrelated and equal power targets with their respective DOA  $13^0$  and  $15^0$ . These curves are plotted for different number of noise eigenvector estimates i.e.  $M = \{1, 2, 3, 4, 5, 6\}$ .

accuracy of the threshold SNR evaluated using the analytical expression in [2] is verified by comparing it with a value obtained through simulations. We use the same simulation parameters as defined in (3.1), (3.3) and (3.4). In Fig. 3.4, the probability of resolution curves, for different values of  $M$ , are obtained at various SNR. These curves are obtained through 50,000 independent trials per SNR for two uncorrelated targets located at  $13^0$  and  $15^0$  respectively. The number of noise eigenvector estimates used is varied from 1 to 6 in this case ( $1 \leq M \leq 6$ ). It can be seen from Fig. 3.4 that the simulated curves crossover at a SNR of 19.1dB ( $\gamma_c$ ). Also, MUSIC offers better resolution performance for low SNR values

when  $M = 1$ . Thus, we can state that the analytical expression in [2] accurately determines the threshold (crossover) SNR.

### 3.1.2 Three Targets

In this section, we discuss the results when three targets are involved but two of them are closely spaced ones. We use the same simulation parameters as defined in (3.3) and (3.4) except for the number of targets ( $K$ ). In this section, the number of targets is 3 ( $K = 3$ ) and the targets are considered as uncorrelated ones having equal power. Correspondingly, the signal covariance matrix ( $\mathbf{R}_S$ ) is defined as

$$\mathbf{R}_S = \begin{bmatrix} 1 & 0 & 0 \\ 0 & 1 & 0 \\ 0 & 0 & 1 \end{bmatrix} \quad (3.8)$$

In Fig. 3.5, the probability of resolution curves are plotted for two targets located at  $13^0$  and  $15^0$  respectively when different number of targets ( $K = 2, K = 3$ ) are involved. These curves are plotted for different values of  $M$  using the expression in [2]. For  $K = 2$ , two targets are located at  $13^0$  and  $15^0$  respectively and the curves are plotted for values of  $M = \{2, 3, 6\}$ . For  $K = 3$ , three targets are located at  $13^0$ ,  $15^0$  and  $30^0$  respectively and the curves are plotted for the values of  $M = \{2, 3, 5\}$ . Both analytical and simulated resolution probability curves have been plotted for the case  $K = 3$ , whereas only analytical ones are plotted for the case  $K = 2$ . It is observed from Fig. 3.5 that the resolution probability curves obtained using (??) for  $K = 3$  approximately matches the corresponding simulated ones obtained through 50000 independent trials. Thus, the expression in [2] accurately predicts the resolution performance of MUSIC in resolving two closely spaced targets in presence of other targets. In addition, we can see that the resolution performance of MUSIC is degraded due to the presence of the third target. Also, the threshold SNR has increased for the case when three targets are involved as compared to the one when only two targets are involved. This effect of the

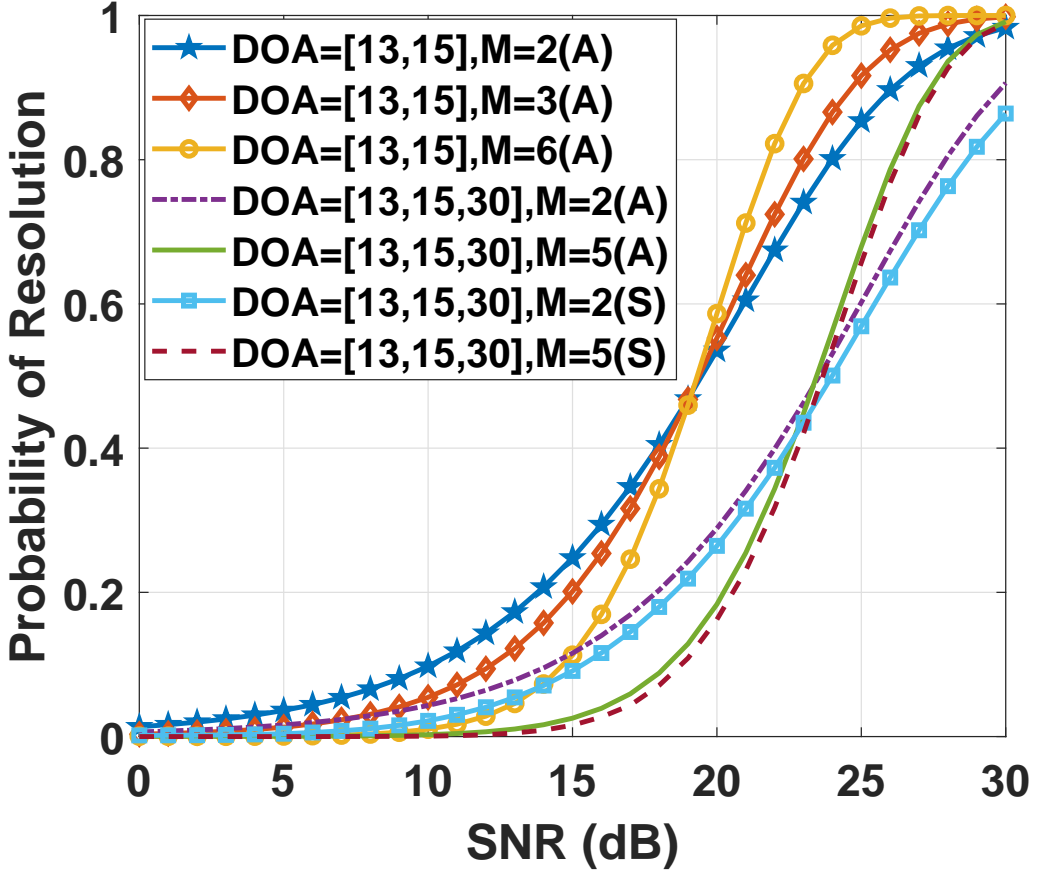


Figure 3.5. Analytical probability of resolution curves plotted for two uncorrelated and equal power targets located at  $13^{\circ}$  and  $15^{\circ}$  respectively for different values of  $M$ , when different number of targets are involved ( $K = 2$  and  $K = 3$ ). (Note: (A) indicates the resolution probability curve obtained analytically using the expression in [2] , whereas (S) indicates the curves are obtained through simulations.)

presence of the third target on the resolution performance of two closely spaced targets fades away as the third target moves farther from the two concerned closely spaced targets.

### 3.2 Experimental Results

The resolution performance of the MUSIC algorithm according to number of noise eigenvectors used have been successfully verified through simulations. But, we want to verify our theoretical findings in a practical scenario by performing real RF experiments. We have per-

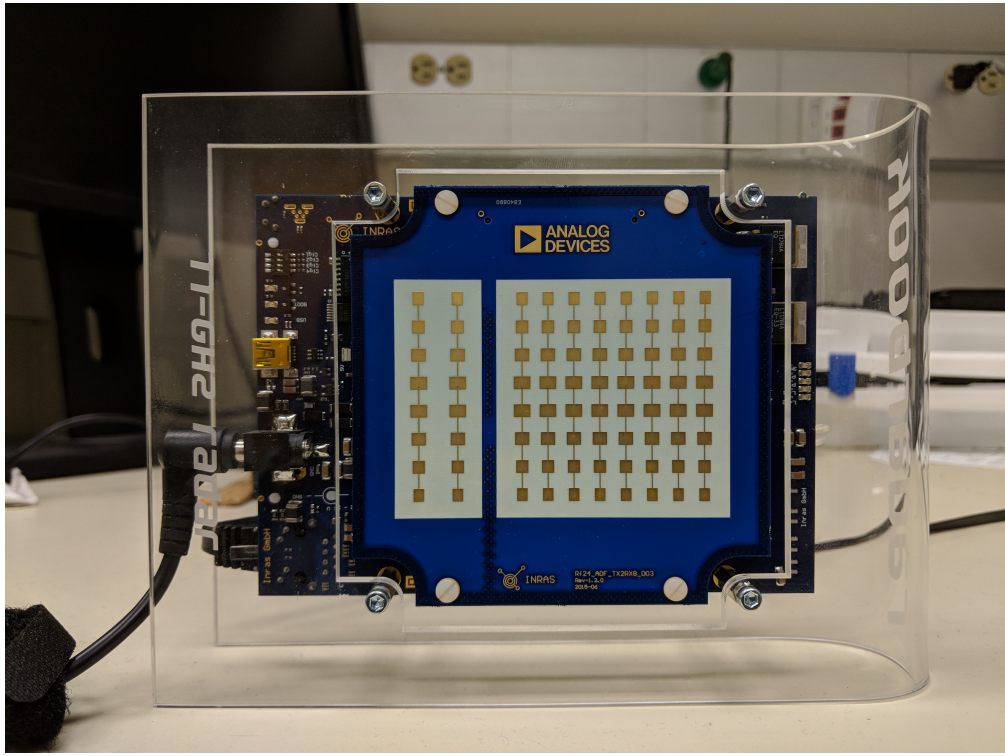


Figure 3.6. 24 GHz antenna array of INRAS Radarbook with 2 Tx and 8 Rx antennas

formed the real RF experiments using a 24-GHz FMCW radar evaluation platform INRAS radarbook [6] to demonstrate the effect of using different number of noise eigenvectors on the resolving capability of MUSIC. The 24-GHz RF frontend of INRAS radarbook as shown in Fig. 3.6 consists of 2 transmit (Tx) antennas and a ULA of 8 receive (Rx) antennas. The FMCW parameters that were used for the experiments are 300 MHz sweep bandwidth, 128  $\mu$ s up chirp duration and 2 MHz sampling rate. We have used two right-angled isosceles trihedral corner reflectors as targets for collecting data with radarbook using 1 Tx and 8 Rx antenna elements. A scenario from our experimental setup can be seen in Fig. 3.7, where two widely separated reflectors were at the same distance from the radar. Both the reflectors were placed at a distance of 4.2 meters from the radar for our experiments. We have performed the far-field measurements for all the real RF experiments presented in this



Figure 3.7. A scenario from the experimental setup with two corner reflectors and INRAS radarbook

section. The resolution performance of MUSIC with the number of noise eigenvectors used was demonstrated through two different experiments that are discussed below.

In the first experiment, the data were collected by varying the angle of separation between the reflectors while keeping the transmit power level of Tx element of the radar fixed at 2.7 dBm. From the analysis perspective, we first apply FFT operation of size 1024 on the collected data samples from a single FMCW chirp measurement across range domain and select the range FFT bin that corresponds to these reflectors. From our initial analysis on the collected data samples, we figured out that the reflectors appeared as correlated targets for some angular separation between them. Thus, we implement a spatial smoothing pre-processing scheme discussed in [3], [17] with a smoothing size of 6 (i.e  $L = 6$ ) on the selected

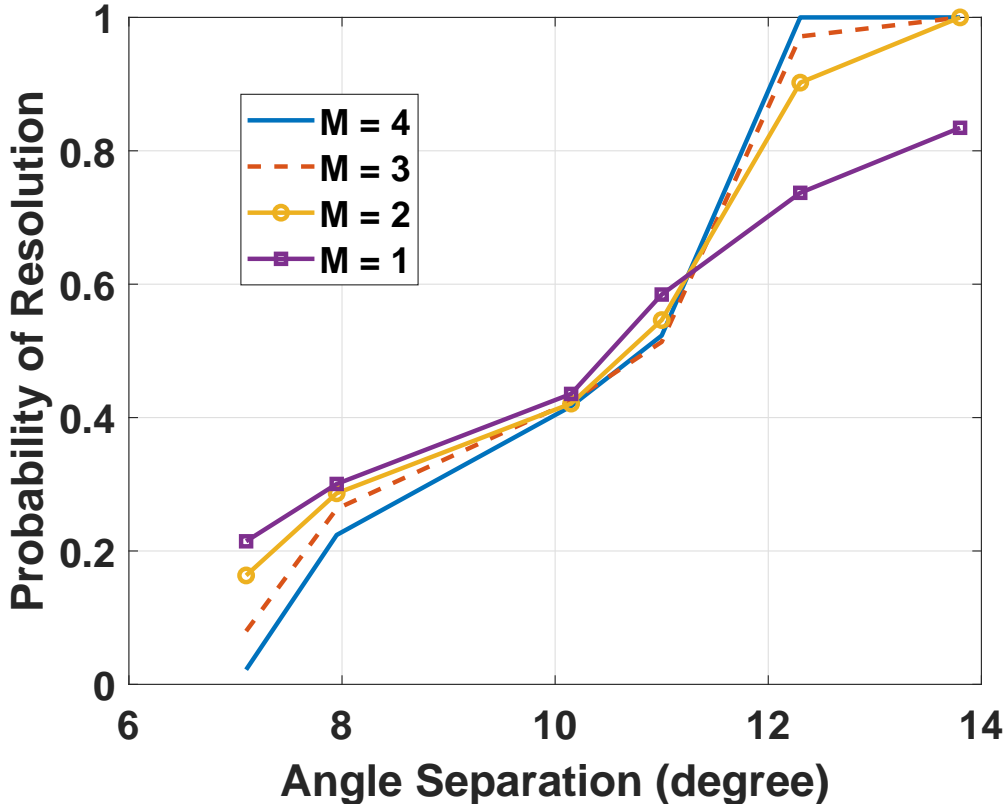


Figure 3.8. Resolution performance of INRAS Radarbook by varying the number of noise subspace eigenvector estimates used across each different angle of separation between two reflectors

FFT range bin data and form the sample covariance matrix. After the implementation of smoothing scheme, we apply MUSIC algorithm to the sample covariance matrix formed in the previous step to determine whether the resolution condition is satisfied or not. This signal processing algorithm applied to the measured data samples is inspired from the algorithm in [14]. In Fig. 3.8, we observe the resolution performance of MUSIC when different number of noise eigenvector estimates are used at various angular separation. The number of available eigenvectors in the noise subspace estimate is 4 ( since  $L=6$ ,  $K=2$  ). The resolution performance is computed for each measurement and the results are averaged over 1000 measurements that were collected for each angle of separation to determine the empirical probability. When  $M$  noise eigenvectors are used in the MUSIC spectrum computation, the

probability of resolution obtained in Fig. 3.8 is the mean of the probabilities computed for all possible sets of  $M$  eigenvectors available in the noise subspace estimate. It can be stated from Fig. 3.8 that a 70% of resolution can be obtained at an angular separation of  $12.5^\circ$  by arbitrarily choosing any one eigenvector from the noise subspace.

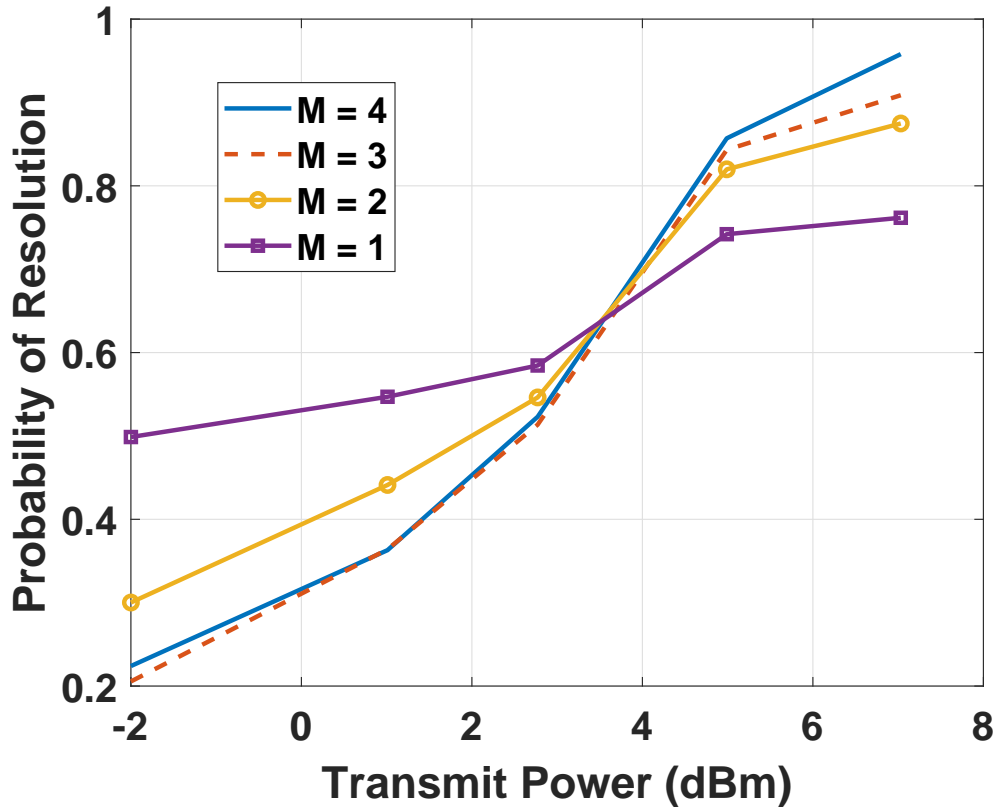


Figure 3.9. Resolution performance of INRAS Radarbook by varying the number of the estimated noise subspace eigenvectors used in MUSIC spectrum computation with respect to varying radar transmit power level.

In the second experiment, the data were collected by varying the transmit power level of the Tx element of the radar while keeping the angle of separation between the reflectors fixed at  $12.5^\circ$ . In order to determine the probability of resolution empirically, we collected 1000 measurements for each transmit power of the radar. The processing algorithm and the approach for computing the probability of resolution are the same as the one used for the previous experiment. Fig. 3.9 compares the resolution performance of MUSIC at

various transmit power levels when the number of noise subspace eigenvectors are varied. The crossover point for this experiment seems to be around the transmit power level of 3 dBm. In Fig. 3.8 and Fig. 3.9, the crossover phenomenon was observed with resolution performance of MUSIC when different number of noise eigenvector estimates were used.

## CHAPTER 4

### TDM MIMO RADAR

In a standard TDM MIMO radar, transmitters are activated sequentially according to their natural spatial order. Due to the relative motion between the radar and a target, the Doppler and DOA information are coupled in the phase sequences of the received signals. As a result, the unambiguous Doppler estimation interval of a standard TDM MIMO radar is reduced by the number of transmit antenna elements as compared to the one in a corresponding SIMO radar. In this dissertation proposal, we formulate the Doppler ambiguity problem associated with a standard TDM MIMO radar.

#### 4.1 FMCW Signal

Frequency modulated continuous wave (FMCW) radars are commonly used for automotive applications. In this chapter, we utilize the FMCW signal model for a standard TDM MIMO radar. The frequency of a FMCW signal varies linearly with time and is given as:

$$f(t) = f_o + \beta t \quad (4.1)$$

where  $f_o$  is the start frequency of the chirp and  $\beta$  is defined as the ratio of the bandwidth of the chirp ( $B$ ) and the chirp duration ( $T_c$ ), i.e  $\beta = B/T_c$ . Then, its instantaneous phase is

$$\psi(t) = 2\pi \int f(t) dt = 2\pi \left( f_o t + \beta \frac{t^2}{2} \right) \quad (4.2)$$

Therefore, the radar signal emitting from a transmitter can be expressed as:

$$x_T(t) = \exp \{ j (2\pi f_o t + \pi \beta t^2) \} \quad (4.3)$$

The received signal is modeled as:

$$x_R(t) = \sum_{i=1}^I \alpha_i \exp \{ j [2\pi f_o (t - \tau_i) + \pi \beta (t - \tau_i)^2] \} \quad (4.4)$$

where

$$i = 1, \dots, I \quad (4.5)$$

$\alpha_i$  is the complex amplitude of the  $i$ th target, whereas  $\tau_i$  is the delay associated with the  $i$ th target. At the receiver, the intermediate frequency (IF) signal is obtained by mixing the received signal  $x_R(t)$  with the transmitted one  $x_T(t)$ .

An example of the standard FMCW TDM MIMO radar with two transmit antenna elements is shown in Fig. 4.1 where  $B$  is the chirp bandwidth,  $T_c$  is the chirp duration,  $T_{int}$  is the chirp repetition interval for a specific transmitter,  $T_{up}$  is the chirp ramp-up duration and  $f_c$  is the carrier frequency.  $T_{int}$  is also regarded as time duration for a single TDM MIMO cycle. In standard TDM MIMO radar, a single TDM MIMO cycle consists of chirps transmitted sequentially from all transmit antennas according to their natural spatial order. For this case, the chirp repetition interval and the chirp duration are related as  $T_{int} = N_T T_c$  where  $N_T$  is the number of transmit antenna elements in TDM MIMO radar.

## 4.2 TDM MIMO: Signal Model

We consider a colocated MIMO radar system where  $N_T$  transmit (Tx) antenna elements and  $N_R$  receive (Rx) antenna elements are uniformly and linearly spaced with an inter-element spacing of  $d_T$  and  $d_R$ , respectively. In this dissertation proposal, we assume 1-D MIMO array radar system for our analysis. After sampling with analog-to-digital converter (ADC), the intermediate frequency (IF) component of the signals, arriving at the  $n$ th receive antenna from  $I$  far-field targets in response to the signal transmitted from the  $m$ th transmit antenna, is approximately modeled as:

$$\begin{aligned} x_{m,n}(l, p) \approx & \sum_{i=1}^I \alpha_i \exp \left\{ j2\pi \left[ \left( \frac{2\beta R_i}{c} + f_{Di} \right) \frac{(l-1)}{f_s} + \frac{(d_{T,m} + d_{R,n})}{\lambda} \sin(\theta_i) \right. \right. \\ & \left. \left. + (m-1)f_{Di}T_c + (p-1)f_{Di}T_{int} \right] + j\phi_i \right\} + w_{m,n}(l, p) \end{aligned} \quad (4.6)$$

$$\text{with } m = 1, \dots, N_T, n = 1, \dots, N_R, i = 1, \dots, I, l = 1, \dots, N_s, p = 1, \dots, N_c \quad (4.7)$$

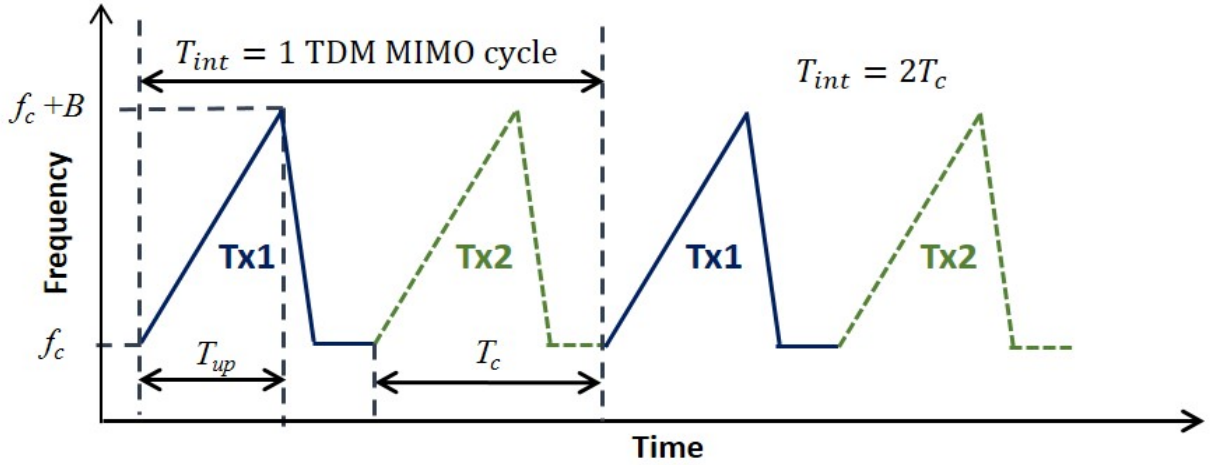


Figure 4.1. An example of a standard TDM MIMO radar with two transmit antenna elements. Frequency modulated continuous wave (FMCW) signals are assumed.

where  $\alpha_i$ ,  $\phi_i$ ,  $R_i$ ,  $\theta_i$  and  $f_{Di}$  are the amplitude, initial phase, range, direction of arrival (DOA) and Doppler frequency, respectively, of the  $i$ th target,  $d_{T,m} = (m - 1)d_T$ ,  $d_{R,n} = (n - 1)d_R$ ,  $\beta (= B/T_{up})$  is the slope of FMCW chirp,  $\lambda (= f_c/c)$  is the wavelength,  $f_s$  is the ADC sampling rate,  $l$  is the fast-time index for ADC samples,  $N_s$  is the number of ADC samples per chirp,  $p$  is the index (slow-time index) for TDM MIMO cycles,  $N_c$  is the number of TDM MIMO cycles required for Doppler measurements and  $w_{m,n}(l,p)$  is additive white Gaussian noise with mean zero and variance  $\sigma^2$ . The Doppler velocity  $v_{Di}$  of the  $i$ th target is related to its Doppler frequency  $f_{Di}$  as  $v_{Di} = \lambda f_{Di}/2$ .

### 4.3 Doppler Ambiguity Problem

In this section, we discuss in detail the problems encountered when a standard TDM MIMO radar is used to estimate the Doppler frequencies and the DOAs of the relatively moving targets. In a standard TDM MIMO radar, the transmitters transmit one at a time according to their natural spatial order. Because of this, in the case of a moving target, an additional phase component, due to the Doppler frequency of the target, is induced in the phase of the received signals. This additional phase component due to the

Doppler frequency is coupled with the phase component containing the DOA information. This coupling phenomenon is observed in the phase of the signal component presented in (2.4). By rearranging the phase terms in (2.4), the coupled phase component is given as  $2\pi \left[ (m - 1) \left( \frac{d_T}{\lambda} \sin(\theta_i) + f_{D_i} T_c \right) + (n - 1) \frac{d_R}{\lambda} \sin(\theta_i) \right]$ . The coupling of the Doppler frequency  $f_{D_i}$  and the DOA  $\theta_i$  of the  $i$ th target will distort the phase of the signals captured by virtual elements and will eventually lead to an inaccurate estimation of the DOA  $\theta_i$ . Therefore, we need to estimate the Doppler frequency  $f_{D_i}$  of the  $i$ th target correctly and compensate it in order to ensure an accurate estimation of the corresponding target DOA  $\theta_i$ . However, the Doppler frequency of the  $i$ th target can be correctly estimated if the actual Doppler frequency  $f_{D_i}$  lies within the limited unambiguous interval  $[-1/(2N_T T_c), 1/(2N_T T_c)]$ . This is because the maximum unambiguously detectable Doppler frequency, i.e.  $f_{D,\max} = 1/(2N_T T_c)$ , for TDM MIMO radar is reduced by the number of transmit antenna elements ( $N_T$ ) in order to satisfy the Nyquist criterion for the Doppler phase shift  $2\pi f_{D_i} N_T T_c$ . If the actual Doppler frequency lies outside the unambiguous interval, then the estimated Doppler will result in ambiguity and will eventually lead to an inaccurate estimation of the target DOA. We present an example of both unambiguous and ambiguous Doppler frequency estimation

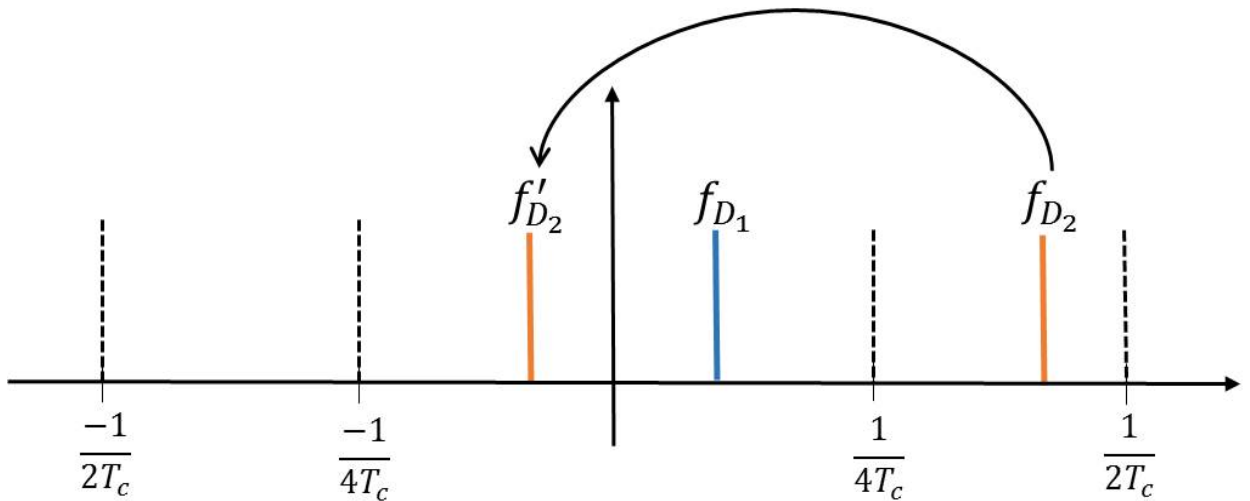


Figure 4.2. Doppler estimation using the standard TDM MIMO radar with  $N_T = 2$

using the standard TDM MIMO radar with  $N_T = 2$  in Fig. 4.2. In this case, the unambiguous estimation interval of Doppler frequencies is  $[-1/(4T_c), 1/(4T_c)]$ . There are two targets ( $I = 2$ ) with Doppler frequencies  $f_{D1} (\in [-1/(4T_c), 1/(4T_c)])$  and  $f_{D2} (> 1/(4T_c))$  that are to be estimated.  $f_{D1}$  will be estimated and compensated accurately as it lies in the unambiguous estimation interval, whereas the estimation of  $f_{D2}$  will result in ambiguity with an incorrect estimation of  $f'_{D2}$ . For this case, the DOA associated with the Doppler frequency  $f_{D1}$  will be estimated precisely, while the one associated with the Doppler frequency  $f_{D2}$  will be erroneously estimated. The inaccurate estimation of the Doppler frequency  $f_{D2}$  can be improved if we can reinstate the limited unambiguous Doppler spectrum estimation interval. Therefore, in this dissertation proposal, we present a signal processing approach for enhancing the reduced unambiguous estimation interval of the Doppler frequencies for a standard TDM MIMO radar. We discuss the signal processing approach in the following section.

#### 4.4 Proposed Idea

We discuss the idea about restoring the unambiguous estimation interval of the Doppler frequencies with an example discussed in section 4.3. From Fig. 4.2, it can be seen that the Doppler frequency  $f_{D2}$  lies in the first Doppler spectral repetition of the unambiguous interval, i.e.  $f_{D2} \in [1/(4T_c), 3/(4T_c)]$ . Thus, the Doppler frequency  $f_{D2}$  can mathematically be expressed as:  $f_{D2} = 2f_{D,\max} + f'_{D2} = \frac{1}{2T_c} + f'_{D2}$  where the maximum detectable Doppler frequency  $f_{D,\max}$  for the standard TDM MIMO radar with  $N_T = 2$  is  $f_{D,\max} = \frac{1}{4T_c}$ . In this case, if the correct Doppler spectral repetition, i.e.  $1/(2T_c)$ , can be determined along with the frequency  $f'_{D2}$ , then the actual Doppler frequency  $f_{D2}$  can be accurately estimated. Therefore, the limited unambiguous estimation interval of the Doppler frequencies can be recovered by correctly determining its spectral repetition for the Doppler frequencies lying outside the unambiguous estimation interval. A concrete solution will be presented in the

dissertation to solve Doppler ambiguity problem associated with a standard TDM MIMO radar.

## CHAPTER 5

### INTERFERENCE MITIGATION IN AUTOMOTIVE RADARS

In this dissertation proposal, we plan to address an interference problem observed with automotive radars.

#### **5.1 Problem Description**

We consider FMCW signal model as they are popular with automotive applications. Automotive radar technology has become a key driver in the recent developments of Advanced Driver Assistance Systems (ADAS) for developing drivers' safety and comfort features. Since modern cars are equipped with ADAS and the transmissions of automotive radars are not synchronized, the occurrence of interference is very likely in dense traffic scenario. This interference might be observed over a very short duration when the interfering signal leaks into the bandwidth of interest for victim radar. Identification of interfering radar will be more challenging when the echoes from strong target masks their transmitted signals. As of now, we focus on the coherence interference problem which occurs when both interfering and victim radars have the same FMCW chirp parameters. To address this problem, a signal processing approach will be proposed to reduce or mitigate the interference in automotive radars.

## CHAPTER 6

### SUMMARY

This dissertation proposal investigates the resolution performance of the MUSIC algorithm according to the number of noise subspace eigenvectors used in the spectrum computation. This investigation cannot be carried out with the existing resolution probability expressions of the MUSIC algorithm. For this purpose, an analytical expression of the resolution probability of the MUSIC algorithm is derived using a statistical framework. The statistical framework, which is presented in this dissertation proposal, is based on the first-order approximation of the perturbations in the noise subspace eigenvectors. Using this framework, a mathematical expression of the resolution threshold in terms of SNR is derived to carry out the resolution threshold analysis of the MUSIC algorithm. The threshold SNR is found to be independent of the number of noise eigenvectors used. The accuracy of the resolution probability expression and the threshold SNR expression is verified with the simulation results. A crossover phenomenon in terms of SNR was observed when we investigated the resolution performances of the MUSIC algorithm with varying number of noise eigenvectors. Also, we found that the resolution probability expression predicts the resolution performance of the MUSIC algorithm for resolving two closely spaced sources in presence of other sources. Such performance predictions cannot be made with the existing probability of resolution expressions. We carried out real RF experiments using a 24 GHz radar platform to verify our theoretical findings in practical scenario. The experimental results confirm the crossover phenomenon of the resolution performances of the MUSIC algorithm when different number of noise eigenvectors are used.

In the latter part of this dissertation proposal, we address a Doppler ambiguity problem associated with a standard TDM MIMO radar. To solve this problem, we will present a cost function to jointly estimate the Doppler frequency and the DOA of targets by restoring the limited unambiguous Doppler spectrum estimation interval to the same level as in SIMO

radar. Also, we describe an interference problem associated with automotive radars in traffic environments with dense target scenario. A signal approach will be proposed to reduce or mitigate the interference.

## REFERENCES

- [1] Barabell, A., J. Capon, D. DeLong, J. Johnson, and K. Senne (1998). Performance comparison of superresolution array processing algorithms. revised. Technical report, Lincoln Laboratory, M.I.T.
- [2] Baral, A. B. and M. Torlak (2019). Impact of number of noise eigenvectors used on the resolution probability of music. *IEEE Access* 7, 20023–20039.
- [3] Evans, J. E., J. R. Johnson, and D. Sun (1982). Application of advanced signal processing techniques to angle of arrival estimation in atc navigation and surveillance systems. Technical report, Lincoln Laboratory.
- [4] Ferreol, A., P. Larzabal, and M. Viberg (2008, May). On the resolution probability of MUSIC in presence of modeling errors. *IEEE Trans. Signal Process.* 56(5), 1945–1953.
- [5] Ferreol, A., P. Larzabal, and M. Viberg (2010, Aug). Statistical analysis of the MUSIC algorithm in the presence of modeling errors, taking into account the resolution probability. *IEEE Trans. Signal Process.* 58(8), 4156–4166.
- [6] Haderer, A. (2013). *INRAS Products-Radarbook*. Linz, Austria: INRAS GmbH.
- [7] Johnson, R. (1986, Aug). Eigenvector matrix partition and radio direction finding performance. *IEEE Trans. Antennas Propag.* 34(8), 985–991.
- [8] Kaveh, M. and A. Barabell (1986, April). The statistical performance of the MUSIC and the minimum-norm algorithms in resolving plane waves in noise. *IEEE Trans. Acoust., Speech, Signal Process.* 34(2), 331–341.
- [9] Lee, H. B. and M. S. Wengrovitz (1990, Sept). Resolution threshold of beamspace MUSIC for two closely spaced emitters. *IEEE Trans. Acoust., Speech, Signal Process.* 38(9), 1545–1559.
- [10] Lee, H. B. and M. S. Wengrovitz (1991, Jun). Statistical characterization of the MUSIC null spectrum. *IEEE Trans. Signal Process.* 39(6), 1333–1347.
- [11] Li, F., H. Liu, and R. J. Vaccaro (1993, Oct). Performance analysis for DOA estimation algorithms: unification, simplification, and observations. *IEEE Trans. Aerosp. Electron. Syst.* 29(4), 1170–1184.
- [12] Li, F. and R. J. Vaccaro (1990, Nov). Analysis of min-norm and MUSIC with arbitrary array geometry. *IEEE Trans. Aerosp. Electron. Syst.* 26(6), 976–985.
- [13] Naha, A., A. K. Samanta, A. Routray, and A. K. Deb (2015, Aug). Determining autocorrelation matrix size and sampling frequency for MUSIC algorithm. *IEEE Signal Process. Lett.* 22(8), 1016–1020.

- [14] Patole, S. M., M. Torlak, D. Wang, and M. Ali (2017). Automotive radars: A review of signal processing techniques. *IEEE Signal Process. Mag.* 34(2), 22–35.
- [15] Rambach, K. (2017). Direction of arrival estimation using a multiple-input-multiple-output radar with applications to automobiles.
- [16] Rambach, K. and B. Yang (2017). Mimo radar: Time division multiplexing vs. code division multiplexing. In *Proc. Int. Conf. Radar Syst.*, pp. 1–5.
- [17] Shan, T.-J., M. Wax, and T. Kailath (1985, Aug). On spatial smoothing for direction-of-arrival estimation of coherent signals. *IEEE Trans. Acoust., Speech, Signal Process.* 33(4), 806–811.
- [18] Stoica, P. and A. Nehorai (1989, May). MUSIC, maximum likelihood, and cramer-rao bound. *IEEE Trans. Acoust., Speech, Signal Process.* 37(5), 720–741.
- [19] Stoica, P. and A. Nehorai (1990, Dec). MUSIC, maximum likelihood, and cramer-rao bound: further results and comparisons. *IEEE Trans. Acoust., Speech, Signal Process.* 38(12), 2140–2150.
- [20] Thomas, J. K., L. L. Scharf, and D. W. Tufts (1995, March). The probability of a subspace swap in the SVD. *IEEE Trans. Signal Process.* 43(3), 730–736.
- [21] Turin, G. L. (1960). The characteristic function of hermitian quadratic forms in complex normal variables. *Biometrika* 47(1/2), 199–201.
- [22] Zatman, M. A. and H. J. Strangeways (1993, Mar). The effect of the number of noise eigenvectors used and quantisation errors on the performance of the music algorithm. In *Proc. IET Eighth Int. Conf. Antennas Propag.*, Volume 1, pp. 481–484.
- [23] Zhang, Q. T. (1995a, April). Probability of resolution of the MUSIC algorithm. *IEEE Trans. Signal Process.* 43(4), 978–987.
- [24] Zhang, Q. T. (1995b, Aug). A statistical resolution theory of the beamformer-based spatial spectrum for determining the directions of signals in white noise. *IEEE Trans. Signal Process.* 43(8), 1867–1873.
- [25] Zhou, C., F. Haber, and D. L. Jaggard (1991, Feb). A resolution measure for the MUSIC algorithm and its application to plane wave arrivals contaminated by coherent interference. *IEEE Trans. Signal Process.* 39(2), 454–463.

## **BIOGRAPHICAL SKETCH**

Ashwin Bhabani Baral received the B.S. degree in Electronics and Electrical Engineering from KIIT University, Bhubaneswar, Odisha, India in 2011. He is currently pursuing the Ph.D. degree in Electrical Engineering at the University of Texas at Dallas, Richardson, TX, USA. His current research focus is on millimeter-wave automotive radars and array signal processing.